Magnetic-field, temperature, geometry, and angle-dependent studies of vortex pinning in vibrating high-T_c superconductor crystals

A. Gupta,* Y. Kopelevich,† M. Ziese, P. Esquinazi, P. Fischer,‡ F. I. Schulz, and H. F. Braun
Physikalisches Institut, Universität Bayreuth, D-95440 Bayreuth, Germany
(Received 22 January 1993)

From the measurement of the resonance frequency and energy dissipation, we have studied the vortex pinning properties of several vibrating high-T_c superconductor crystals $YBa_2Cu_3O_7$, $Bi_2Sr_2CaCu_2O_{8+x}$, and oxygen-reduced Y(6% Gd)$Ba_2Cu_3O_{6.83}$. We have studied the response of the crystals under magnetic field ($0\ T \leq B \leq 8\ T$), temperature ($10\ K \leq T \leq 120\ K$), angle between field and CuO_2 planes ($0° \leq \theta \leq 90°$), and for different geometrical arrangements and driving forces. We can understand the enhancement of the resonance frequency with field taking into account the geometry of the crystals and their orientations. In a certain temperature and field range our results indicate that "Josephson vortices" in $Bi_2Sr_2CaCu_2O_{8+x}$ remain pinned. At angles $0° < \theta < 90°$ we have measured double dissipation peaks in all the crystals investigated. This effect can be quantitatively understood with the thermally activated depinning and vortex diffusion model using resistivity data from literature. We discuss briefly unique dissipation features measured in Y- and Bi-based superconductors.

I. INTRODUCTION

The irreversibility or depinning line (DL) in the magnetic-field–temperature (B-T) plane delineates an effectively pinned from a thermally activated depinned flux-line lattice (FLL).[1–9] Because of a relatively low activation barrier U_b for pinning of the layered high-T_c superconductors (HTS's),[2,10,11] the action of low driving forces aided by thermal activation leads to a diffusive response of the FLL to magnetic-field perturbations.[7,9,12,13] With ac techniques, a peak in the energy dissipation occurs if the FLL diffuses just the relevant length of the sample within one cycle of the driving force, provided the wavelength of the periodic perturbation is larger than the sample dimensions.[7–9,12,13] With the exception of ultrasound techniques,[14,15] this case is always achieved in typical ac experiments.

Recent theoretical work[16–22] and experimental results[23–27] indicate the existence of phase transitions of different kinds of the FLL in HTS compounds. These results incite further investigation. In particular, measurements as a function of angle between the magnetic-field and CuO_2 planes are of interest because they may reveal whether the observed anomalies are due to vortex diffusion or a phase transition of the FLL.

In this paper we present systematic measurements of damping and frequency enhancement for Bi 2:2:1:2, Y(Gd 6%) 1:2:3 and Y 1:2:3 single crystals vibrating in an applied magnetic field. Different vibration configurations and field orientations with respect to CuO_2 planes, varying reed amplitude, and a broad field range (0.01–8 T) have been used to probe the B-T plane. The advantages of the vibrating-reed technique for the study of the dynamical response of the FLL and the elastic pinning of the FLL are based on the very low effective ac fields ($\leq 0.1\ \mu T$ for typical reed amplitudes) generated by tilting the reed. This very small ac field generates very small shielding currents (I) on the surface of the superconducting sample, e.g., $I/\lambda < 1\ A/m^2$ for $B = 1$ T and a reed amplitude of $\sim$10 nm (Ref. 28) (λ is the magnetic-field penetration depth). The small currents which mean small driving forces enable the study of the response of the FLL in the zero-current limit as revealed by the reed-amplitude independence of the anomalies at the thermally activated depinning. They can be interpreted within the thermally assisted flux-flow TAFF model.[7]

The main objectives of this work are the following.

(1) We discuss theoretically and experimentally the resonance-frequency enhancement as a function of magnetic field for a superconducting slab performing oscillations in different configurations. Based on such measurements on a Bi 2:2:1:2 crystal, we elucidate that even in quasi-two-dimensional (quasi-2D) superconductors the flux lines (FL's) $\parallel$ CuO_2 planes ("Josephson vortices") are pinned and oscillate along with the crystal. We find that the field dependence of the resonance frequency indicates a tilt-modulus contribution as well as an elastic-coupling contribution depending on the field orientation and the sample size.

(2) Recently, two distinct peaks in the dissipated energy as a function of temperature were observed in a series of ac experiments and on different superconducting samples. This interesting phenomenon was reported for HTS's,[25,29] an organic superconductor,[30] Nb and Nb_2Se,[31] and Mo-Ge films.[32] The dissipation peaks were interpreted in terms of thermally activated depinning and vortex diffusion in Refs. 25 and 30 and a quantitative treatment was developed recently for 3D-anisotropic superconductors by Brandt[33] based on thermally activated depinning and vortex diffusion. We show that such dou-

ble peaks are generic to both Bi- and Y-based superconductors. The origin of the double peak is geometric and is shown to be consistent with the diffusive motion of FLL's, which gives rise to a skin depth for the small probing ac field which penetrates along different dimensions of the vibrating slab. We also show that the angular scaling of the characteristic peak temperature with field in layered superconductors is a direct consequence of the scaling of resistivity observed in these materials.[34–37] The recent scaling model suggested for double peaks in 3D-anisotropic superconductors[33] is compared with experimental results obtained on fully oxygenated Y-based HTS's.

(3) In the limit of low driving forces, the TAFF model predicts reed-amplitude-independent dissipation peaks. We investigate the linearity of the dissipation peaks in all three Bi 2:2:1:2, low-oxygen-content Y(Gd 6%) 1:2:3 and fully oxygenated Y 1:2:3 systems with $B \perp CuO_2$ planes.

The work is further divided into six more sections. In Sec. II the experimental and sample details are given. In Sec. III we discuss theoretically the expected frequency enhancement as a function of field and the response of vibrating superconductors when the FLL is thermally activated depinned. In Sec. IV we present the experimental results. The damping and frequency enhancement as a function of temperature and magnetic field for both Y- and Bi-based crystals with applied field at different angles with respect to CuO_2 planes are shown. A comparison of the DL's for all compounds, taking into account the field orientation with respect to CuO_2 planes, with constant resistivity lines is shown. We also compare the activation barriers in all the three compounds. In Sec. V the amplitude dependence of the damping and its peak temperature and the resonance frequency for applied-field $B \perp CuO_2$ planes in Bi- and Y-based crystals are presented. A short discussion of the recently observed anomalous behavior of the FLL is given in Sec. VI. We summarize the results and interpretations in Sec. VII.

II. EXPERIMENTAL DETAILS

We performed extensive measurements of the resonance-frequency enhancement in a magnetic field $\Delta\nu = \nu(B,T) - \nu(0,T)$ and excess damping $\Gamma = \Gamma(B,T) - \Gamma(0,T)$ of single crystals of high-temperature superconductors attached to a dielectric vibrating reed. The experimental setup has been described in detail in Ref. 38. Measurements were taken both isothermally as a function of magnetic field B and as a function of temperature T at fixed field. In all measurements a small crystal was glued with vacuum grease to a host reed, fabricated from polymer resin or MgO crystals with typical reed dimensions of 8–12 mm $\times$1–2 mm$\times$100–200 μm $= L \times w \times d$ and covered with a gold layer (typically $\simeq$ 40 nm) on both surfaces. Without the crystal, there was no significant magnetic-field dependence from the host reed.

We used three configurations, designated conf.1, conf.2, and conf.3, in which the superconducting single-crystal platelet of length L_p, width w_p, and thickness d_p ($L_p, w_p > d_p$; the crystallographic c axis is perpendicular to the large face) is attached to the vibrating host reed [see Figs. 1(a)–1(c)]. The thickness of the superconducting crystal d_p is oriented along the y axis in conf.1, x axis in conf.2, and z axis in conf.3. The host reed vibrates in the z,y plane, which causes a tilt oscillation of the sample about the x axis with a small angular amplitude ($\phi < 10^{-5}$ rad). Angle-dependent measurements were performed in conf.1 [Fig. 1(a)], with the reed holder rotated about the x axis by a fixed angle θ. Note that θ represents the angle between the CuO_2 planes and the applied field with the reed at rest. Reed-amplitude-dependent measurements were performed in conf.3 [Fig. 1(c)] with $B \perp CuO_2$ planes. All the measurements have been done cooling the sample through the critical temperature in an applied magnetic field, i.e., field cooled.

We present results on five different single crystals: two $Bi_2Sr_2CaCu_2O_{8+x}$ (BSC1, $2 \times 0.9 \times 0.02$ mm^3; BSC2, $1.8 \times 1 \times 0.025$ mm^3), one Y(6% Gd)$Ba_2Cu_3O_{6.83}$ (YGBC1, $1.7 \times 0.25 \times 0.025$ mm^3), and two $YBa_2Cu_3O_7$ (YBC1, $0.65 \times 0.65 \times 0.2$ mm^3; YBC2, $0.8 \times 0.8 \times 0.25$) crystals. Details on the preparation by flux growth and characterization has been given elsewhere.[39–41] The crystals used in this work were optically free from flux, and their stoichiometry and crystalline structure was confirmed by microprobe and x-ray analysis. Some of the crystal surfaces were studied with scanning tunneling microscopy.[41]

Figure 2 shows ac-susceptibility curves for the BSC2, YGBC1 and YBC1 crystals obtained at zero dc applied field. The width of the transition as well as the observed inflexions in the ac-susceptibility curve for the BSC2 crystal depend sensitively on the amplitude of the ac field; these features might be due to a geometrical effect (field misalignment) as revealed by the vibrating-reed measurements. The inset of Fig. 2 shows the temperature dependence of the electrical resistance of the

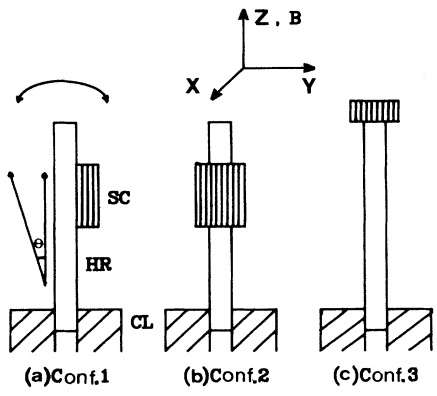

FIG. 1. Schematic of the nonconducting host reed (HR) with an attached small superconducting crystal platelet (SC) corresponding to configurations (a) conf.1, c axis $\parallel y$; (b) conf.2, $c \parallel x$; (c) conf.3, $c \parallel z$. θ represents the angle between applied field B and the reed at rest. CL: Clamp.

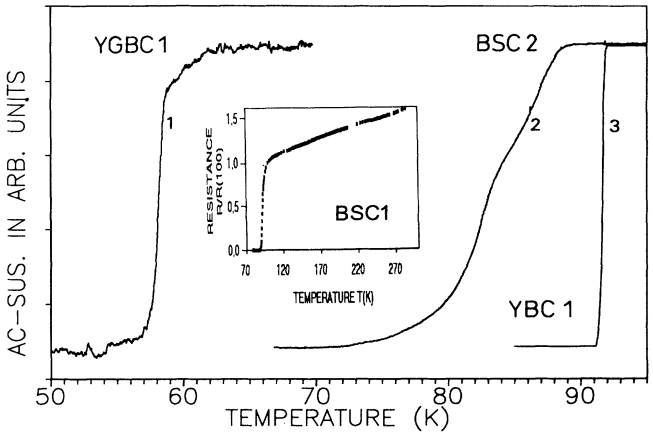

FIG. 2. Superconducting transition curves of (1) Y(6% Gd)$Ba_2Cu_3O_{6.83}$ (YGBC1), (2) $Bi_2Sr_2CaCu_2O_{8+x}$ (BSC2), and (3) $YBa_2Cu_3O_7$ (YBC1) single crystals measured by ac susceptibility with an ac field applied perpendicular to the CuO_2 planes. Inset: electrical resistance as a function of temperature for the BSC1 crystal.

crystal BSC1 for currents parallel to the CuO_2 planes obtained with the four-probe method at zero field.

The superconducting transition temperatures as determined from the onset of the excess dissipation in the vibrating-reed experiment (conf.1) with $\theta = \pm 0.4°$ and $B \leq 1000$ G are 90.5 K for both Bi-based crystals, 67.0 K for YGBC1, and 90.5(91.0) K for YBC1 (YBC2).

III. THEORY

A. Frequency enhancement in a magnetic field

We consider an applied magnetic field $B \gg B_{c1}$, such that the static magnetization can be neglected and the applied field is nearly equal to the field inside the superconducting platelet. In general, the resonance frequency of a vibrating superconductor in a magnetic field increases as a result of an extra magnetic line tension pulling along the reed.[28,42–44] Depending on the geometry of the reed arrangement, this extra line tension can be attributed to surface-shielding currents, the FLL tilt modulus, and the elastic pinning force between the FLL and pinning sites. Below we give expressions for the line tension appropriate for the different configurations shown in Figs. 1(a)–1(c).

In conf.1 [Fig. 1(a)], if $L_p/2 \gg (\pi w_p/4d_p)\lambda_{44}$ [where $\lambda_{44} = (c_{44}/\alpha)^2$ is the tilt penetration depth,[42] c_{44} the FLL tilt modulus, and α the Labusch parameter], the line tension P_1 arises from the surface currents generated on the main surface of the crystal due to the shielding of the small ac-field component created when the reed tilts by a small angle ϕ in the magnetic field. P_1 will be given by the same expression as derived for a bulk superconducting reed in Ref. 42, except that it will be reduced by a geometrical factor $w_p^2 L_p/w^2 L$, i.e.,

$$P_1 = \pi(w_p/2)^2 c_{44} L_p/L. \tag{1}$$

The factor L_p/L takes into account the reduction of the tilt energy due to the smaller length of the superconducting crystal. The tilt modulus of the FLL for isotropic superconductors and in the long-wavelength limit (local approximation) is

$$c_{44} = B^2/\mu_0. \tag{2}$$

According to Brandt and Sudbø this expression for the tilt modulus should hold also for anisotropic superconductors in not too small fields $B > B_{c1}$ for the Ginzburg-Landau parameter $\kappa > 2$.[45]

A second, usually smaller contribution due to the tilt modulus of the FLL becomes important in conf.2 [Fig. 1(b)], where the shielding contribution can be neglected when the condition $w_p \gg d_p$ holds. If $L_p/2 \gg \lambda_{44}$ in conf.2 or $d_p/2 \gg \lambda_{44}$ in conf.3, the line tension is

$$P_2 = w_p d_p c_{44} L_p/L. \tag{3}$$

If $L_p/2 \leq \lambda_{44}$ in conf.2, then the line tension will be proportional to the elastic coupling constant α between the FLL and pinning centers:

$$P_3 = w_p d_p \alpha g L_p/L. \tag{4}$$

Here g is a geometrical factor which depends on the shape of the platelet. For a parallelepiped platelet in conf.2, $g = L_p^2/3$. The line tension P_3 in the configuration conf.3 [Fig. 1(c)] will have an origin similar to that of conf.2, except that the relevant dimension to be compared with λ_{44} is now d_p and thus $g = d_p^2/3$.

For a volume ratio of the crystal to the host reed, $f \ll 1$, we can approximately represent the frequency enhancement in the three configurations by the following relation:

$$\omega^2(B) - \omega^2(0) \approx 4.65 P_i/(\rho_h d w L^2), \tag{5}$$

where P_i is the line tension relevant for a particular configuration i and ρ_h is the density of the host reed ($\omega = 2\pi\nu$).

If the measurement is done in conf.1 and $L_p/2, d_p/2 \gg \lambda_{44}$, the line tension P_i is angle dependent and is given by

$$\begin{aligned} P_i(\theta) &= P_1 \cos^2(\theta) + P_2 \sin^2(\theta) \\ &= (\pi w_p^2 c_{44} L_p/4L)[\cos^2(\theta) + (4d_p/\pi w_p)\sin^2(\theta)]. \end{aligned} \tag{6}$$

The functional dependence on $\cos^2(\theta)$ and $\sin^2(\theta)$ is valid if the tilt modulus $c_{44} \propto B^2$ and represents the field components parallel and perpendicular to the main surface of the crystal in conf.1.

B. Thermally activated depinning in anisotropic HTS's

For small driving forces, the high-temperature superconductors show a linear resistivity due to thermally ac-

tivated flux flow (TAFF) in a broad temperature regime below T_c:

$$\rho(B,T,\theta) \simeq \rho_{\rm FF} \exp\left[-U_b(B,T,\theta)/kT\right], \tag{7}$$

where $\rho_{\rm FF}$ is the flux-flow resistivity and U_b is an effective activation barrier for vortex motion.

Let us consider a perfectly rectangular crystal platelet aligned as shown in Fig. 3, oscillating about the x axis with angular amplitude ϕ in a magnetic field B inclined at an arbitrary angle $0° < \theta < 90°$ in the y,z plane. Because of the periodic oscillations, an ac-field component is generated perpendicular to the sets of parallel faces A, C, with amplitude $b_A, b_C \ll B$ and frequency ω, the resonance frequency of the vibrating reed. If the third crystal face is not aligned perpendicular to the oscillation axis, an ac field b_B normal to it will be present.

Within the TAFF model, the penetration of the ac field into the crystal is governed by FLL diffusion with a diffusivity $D = \rho/\mu_0$, which in an anisotropic medium will depend on the direction of the flux motion. In the general case discussed above, we have three diffusion modes[33] which give rise to three different skin depths:

$$\delta_i = (2D_i/\omega)^{1/2} = [2\rho_i(B,T,\theta)/(\mu_0\omega)]^{1/2}. \tag{8}$$

At fixed B and θ, the skin depth increases with $D_i(B,T,\theta)$ at increasing temperature. At some characteristic value of $D_i(B,T_{Di},\theta)$, at the so-called depinning temperature T_{Di}, δ_i becomes of the order of the relevant dimension l_i of the crystal (different for each mode) and a peak in dissipation accompanied with a step in frequency enhancement is observed. At a fixed angle, each mode gives rise to a depinning line (DL) as a function of applied field $T_{Di}(B,\theta)$, which is equivalent to a line of constant resistivity for

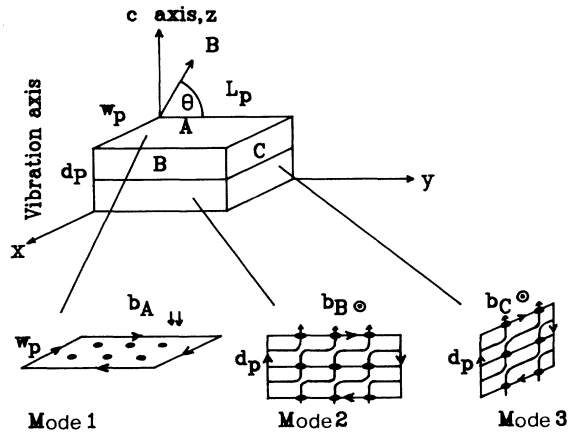

FIG. 3. Upper part: vibrating superconducting slab, with magnetic field oriented at an arbitrary angle θ with respect to CuO_2 planes. Lower part: three possible diffusion modes as viewed from the three faces of the slab with point vortices of density $B\sin\theta$ along with the ac-field components b_A, b_B, and b_C. The arrows on the edges indicate the flow of currents generated by the ac-field components.

$$\rho_i(B,T_{Di},\theta) \simeq \omega l_i^2 \mu_0/\pi^2. \tag{9}$$

If the relevant dimension for each mode is known, then the measured DL can be compared with the corresponding constant resistivity line.

1. 2D superconductors

We first discuss the relevant resistivity and dimension in each mode for highly anisotropic Bi 2:2:1:2. According to Kes *et al.*,[34] in a field B inclined an angle θ with respect to the CuO_2 planes, the perpendicular component penetrates in the form of point ("pancake") vortices with a density $B\sin\theta$, and the field component parallel to the planes penetrates the crystal without forming Abrikosov vortices. In mode 1, the currents which shield the ac field generate a compression on the point vortices, which diffuses along the width or length of the crystal (see Fig. 3). The relevant resistivity is the in-plane resistivity ρ^c_{ab} (upper indices characterize the field direction, lower indices the current direction) due to the point vortices. The damping peak is due to the ac-field penetration along the smaller dimension, the width w_p (once the field has entered along w_p, it need no longer penetrate along L_p).

In mode 3, the currents along the thickness are in a force-free configuration with respect to the point vortices, whereas the currents along the width of the crystal generate a "tilt" of the point vortices, which penetrates the crystal along the thickness d_p (see Fig. 3). In mode 2, present if $b_B \neq 0$, the situation is just as in mode 3, with the role of length and width interchanged. The relevant resistivity in both these modes is again the in-plane resistivity ρ^c_{ab} and the ac field penetrates along the thickness d_p. Since mode 2 and mode 3 are equivalent, they will not give rise to separate dissipation peaks, and at any arbitrary angle $0° < \theta < 90°$ only two peaks in the dissipation will be observed. The penetration of an ac field into a Bi 2:2:1:2 crystal will thus be governed in all modes by the motion of the point vortices due to the $B\sin\theta$ component and only the linear in-plane resistivity ρ^c_{ab} data is required for comparison with a DL. Indeed, the resistivity ρ^θ_{ab} in these layered quasi-2D compounds scales with $B\sin\theta$,[35–37]

$$\rho^\theta_{ab}(B,T,\theta) = \rho^c_{ab}(B\sin\theta,T) \tag{10}$$

for $\theta \geq 5°$. Recent vibrating-reed measurements indicate that this scaling holds to smaller angles as well.[25] Thus, for all modes, the depinning line $T_{Di}(B,\theta)$ should scale with $B\sin\theta$. We would like to mention here that the frequency enhancement in these modes at temperatures less than T_{Di} can have different contributions, as will be shown in Sec. IV A.

In the light of the recent observation[46,47] of much higher Arrhenius resistivity ρ^c_c, i.e., when the field is applied along the c axis and the measuring current flows along the c axis in a force-free configuration, the faster diffusion could occur along L_p in mode 2 and along w_p in mode 3 (see Fig. 3) in thicker crystals instead of along d_p. Note that both these modes are not equivalent due to

different dimensions involved and one expects then *three* dissipation peaks. Since the dissipation mechanism for this configuration is not clear at present, we postpone a further empirical discussion to Sec. IV B.

2. 3D-anisotropic superconductors

We now turn to the fully oxygenated $YBa_2Cu_3O_7$, which should be treated as uniaxial anisotropic 3D system. As shown recently by Brandt,[33] in each mode the anisotropic diffusivity D is related to the in-plane diffusivity D^c_{ab}:

$$\begin{aligned} &\text{mode 3.1}: \quad D_{3.1} = (\epsilon/\gamma) D^c_{ab}(B\epsilon/\gamma, T); \\ &\text{mode 3.2}: \quad D_{3.2} = (\epsilon/\gamma) D^c_{ab}(B\epsilon/\gamma, T); \\ &\text{mode 3.3}: \quad D_{3.3} = (\gamma/\epsilon) D^c_{ab}(B\epsilon/\gamma, T). \end{aligned} \tag{11}$$

Here $\epsilon^2 = \cos^2\theta + \gamma^2 \sin^2\theta$ and $\gamma = \lambda_c/\lambda_{ab} = (m_c/m_{ab})^{1/2}$ is the anisotropy ratio. In mode 3.2 and mode 3.3, the penetrating ac field is directed along the c axis and the motion is along the width or the length. These modes can be compared with mode 1 as discussed above for $Bi_2Sr_2CaCu_2O_{8+x}$. In Brandt's mode 3.1, the ac field is perpendicular to c and the diffusion is along c; this can be compared to our mode 3 above. Since for the configuration considered in Ref. 33 the field B and the c axis lie perpendicular to the vibration axis, our mode 2 will be absent. The relevant dimensions are as follows:[33]

$$\begin{aligned} &\text{mode 3.1}: \quad l_{3.1} = d_p; \\ &\text{mode 3.2}: \quad l_{3.2} = \sqrt{L_p^2 4 d_p/(\pi w_p)}; \\ &\text{mode 3.3}: \quad l_{3.3} \simeq \sqrt{w_p d_p/\sin^2\theta}. \end{aligned} \tag{12}$$

According to Brandt, for a large range of angles $|\sin\theta| > (\pi/4)^{1/2}(w_p/L_p)(\epsilon/\gamma)$, mode 3.3 will be faster than mode 3.2 and will cause the depinning peak. At $|\sin\theta| = (\pi/4)^{1/2}(w_p/L_p)(\epsilon/\gamma)$ both modes coincide.

If the layered nature in the $YBa_2Cu_3O_7$ crystal is relevant, it would lead to a 2D vortex array similar to the Bi 2:2:1:2 system. The relevant dimensions for mode 1 and mode 3 will be w_p and d_p as shown for Bi 2:2:1:2 in Fig. 3. Indeed, down to angles $\theta \simeq 15°$ the resistivity ρ^θ_{ab} scales as $B\sin\theta$.[35] Below this angle a 3D-anisotropic scaling

$$\rho^\theta_{ab}(B, T, \theta) = \rho^c_{ab}(B\epsilon/\gamma, T) \tag{13}$$

is plausible.[35,48,49] Note, however, that for higher angles Eqs. (10) and (13) are indistinguishable.[35] The dissipation peak temperatures due to the two diffusion modes are then expected to scale approximately as $B\epsilon/\gamma$ for all angles if the 3D-anisotropic approach is correct.

IV. EXPERIMENTAL RESULTS

A. Frequency enhancement in a magnetic field

1. Y(6% Gd)$Ba_2Cu_3O_{6.83}$ single crystal

Figure 4 shows the measured frequency enhancement $\omega^2(B) - \omega^2(0)$ as a function of applied magnetic field B at fixed temperature and in different configurations for the YGBC1 and BSC1 crystals.

For the YGBC1 crystal we estimate $\lambda_{44} = (c_{44}/\alpha)^{1/2} = 32$ μm at 20 K and $B = 1$ T using Eq. (2). The value of α is taken from measurements on the same crystal for $B \parallel CuO_2$ planes.[50] In conf.2, the condition $\lambda_{44} = 32$ μm $\ll L_p/2 = 0.85$ mm is easily fulfilled and indeed the observed $\omega^2(B) - \omega^2(0) \propto B^2 \propto c_{44} \propto P_2$.

In conf.3 ($B \perp CuO_2$ planes) nearly the same frequency enhancement $\omega^2(B) - \omega^2(0) \propto B^2$ as in conf.2 is observed. This indicates a tilt-modulus contribution to the frequency enhancement in conf.3. Using Eq. (5) and the appropriate line tension P_2 [Eq. (3)] for both conf.2 and conf.3, we can fit the frequency enhancement as a function of field for both configurations (solid line in Fig. 4) without free parameters. However, since $d_p/2 = 12.5$ μm for the YGBC1 crystal, $\lambda_{44}(B \perp CuO_2$ planes) is required to be $< \lambda_{44}(B \parallel CuO_2$ planes) $= 32$ μm. This is possible since λ_{44} in anisotropic superconducting crystals can be different for a different field direction and is determined by the value of α in the particular direction. A deviation from a B^2 dependence results at high fields (see Fig. 4) when thermally activated depinning becomes important.

2. $Bi_2Sr_2CaCu_2O_{8+x}$ single crystal

For the BSC1 crystal in conf.2 ($B \parallel CuO_2$ planes) we again find $\omega^2(B) - \omega^2(0) \propto B^2$ (Fig. 4). In contrast, in

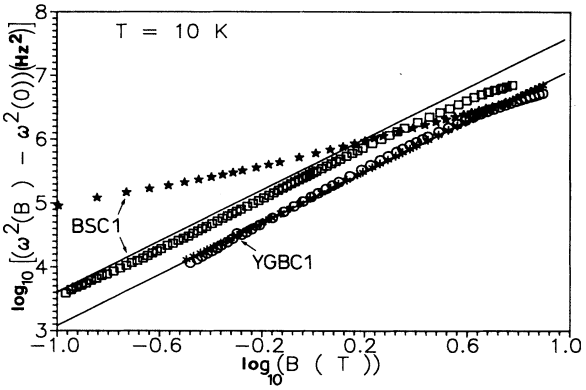

FIG. 4. Resonance-frequency enhancement as a function of magnetic field at a fixed temperature of 10 K for single crystals Y(6% Gd)$Ba_2Cu_3O_{6.83}$ (YGBC1): (*) conf.2, (○) conf.3; and $Bi_2Sr_2CaCu_2O_{8+x}$ (BSC1): (□) Conf.2, (*) Conf.3. The solid lines represent the frequency enhancement calculated after Eqs. (2), (3), and (5).

conf.3 ($B \perp CuO_2$ planes), the frequency enhancement shows nearly linear behavior with field (Fig. 4). This B dependence in conf.3 certainly indicates that the line tension is not dominated by $c_{44} \propto B^2$, but is proportional to the elastic coupling α. The crossover of the field dependence of the resonance frequency from a tilt-modulus to an elastic-coupling contribution can be seen in Fig. 5. The data in Fig. 5 have been obtained in conf.1 at different angles between field and CuO_2 planes and at $T = 60$ K. We note that the dependence of $\omega^2(B) \propto B^n$ changes from an exponent $n = 2.0$ for $\theta \leq 15°$ to $n \simeq 1$ for $\theta \geq 75°$. For a given angle, $\omega^2(B)$ flattens at high enough fields due to thermally activated depinning (see Sec. IV B 1).

One could also argue that $c_{44} \propto B$ for Bi 2:2:1:2 crystals if the point vortices are treated as independent or isolated (single) vortices[51] (for angles where no shielding contribution is expected). However, this tilt-modulus contribution cannot explain our data. Note that the frequency enhancement in conf.3 at $B < 1$ T is larger than in conf.2 (Fig. 4). If $c_{44} \simeq BH_{c1}$ for isolated vortices,[51] we have to assume a lower critical field $H_{c1}(B \perp CuO_2) \geq 10^4$ Oe in order to fit the data which is much larger than any reasonable value taken from literature.[52]

With the known dimensions of the crystal and the expression for P_3 in Eq. (5), we obtain for $T = 10$ K and $B = 1$ T values for $\alpha = 1.6 \times 10^{15}$ N/m^4 and $\lambda_{44}(B \perp CuO_2) = 22$ μm. This value of λ_{44} is smaller than the 130 μm obtained for a Bi-based polycrystalline sample measured in Ref. 43. However, $d_p/2 = 10$ μm $< \lambda_{44} = 22$ μm $\ll L_p/2 = 1$ mm, which is in good agreement with the observed variation of $\omega^2(B) - \omega^2(0) \propto B^2 \propto c_{44} \propto P_2$ for conf.2 (see also below) and $\omega^2(B) - \omega^2(0) \propto \alpha(B)$ for conf.3.

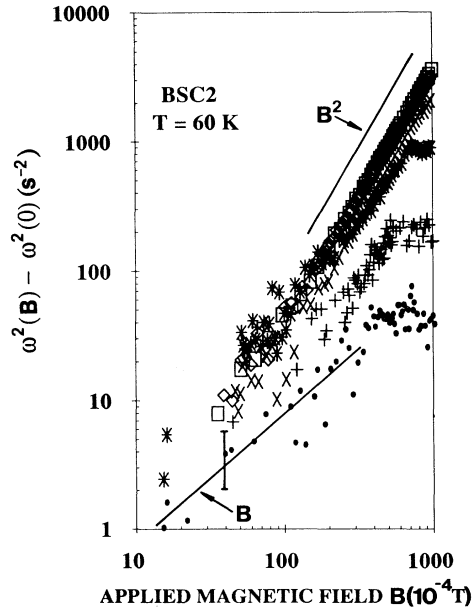

FIG. 5. Frequency enhancement as a function of the applied field for the $Bi_2Sr_2CaCu_2O_{8+x}$ (BSC2) crystal at $T = 60$ K and at different angles between field and CuO_2 planes: (•) 75°, (+) 60°, (*) 45°, (×) 30°, (◇) 15°, (□) 0°. The straight lines are only a guide.

For the BSC1 crystal in conf.2, according to the model of Kes *et al.*,[34] the magnetic field penetrates the space between CuO_2 planes without forming an Abrikosov lattice. Interestingly, our measurements in this configuration for the BSC1 crystal show a large frequency enhancement $\propto B^2$ (Fig. 4). The contribution related to Abrikosov vortices generated perpendicular to the CuO_2 planes by a misalignment angle between applied field and CuO_2 planes in conf.2, estimated to be $\leq 3°$, would be far too small ($\leq B^2 \sin^2 3°$) to produce the observed large frequency enhancement. Further, the surface currents in the x, z plane are negligible because of the extremely small crystal thickness. The frequency enhancement can only be understood assuming a c_{44} contribution from the field in the interplanar region. This component of the magnetic field would penetrate the superconductor as "Josephson vortices" or "Josephson strings."[21,53]

Assuming that the Josephson vortices $\parallel CuO_2$ planes are pinned and contribute to the frequency enhancement, we get a good agreement between the results of conf.2 and the frequency enhancement calculated using Eq. (5) and the line tension P_2 [Eq. (3)] (solid line in Fig. 4). The small discrepancy between the theoretical line and the experimental points can be understood assuming weak pinning in Bi 2:2:1:2.

3. *$YBa_2Cu_3O_7$ single crystal*

Figure 6 shows the measured frequency enhancement $\omega^2(B = 1.4\text{T}) - \omega^2(B = 0)$ as a function of angle between field and CuO_2 planes at $T = 80$ K for the YBC1 crystal. The continuous line was calculated according to Eqs. (5) and (6) taking into account the geometry of the crystal. The agreement between theory and experiment indicates that the frequency enhancement is due to the tilt-modulus c_{44} contribution, which changes with angle due to the sample geometry. A similar angular dependence was observed for the dynamic torque on an untwinned $YBa_2Cu_3O_7$ crystal.[27]

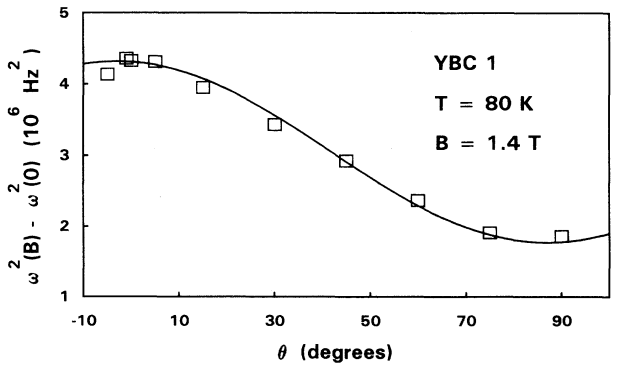

FIG. 6. Frequency enhancement as a function of angle between field and CuO_2 planes at $B = 1.4$ T and $T = 80$ K for the YBC1 crystal. The continuous line was obtained after Eqs. (1)–(6) with a geometrical factor $4d_p/\pi w_p = 0.41$ (measured value 0.39 ± 0.04).

B. Thermally activated depinning

1. $Bi_2Sr_2CaCu_2O_{8+x}$ single crystal

In Fig. 7, we show the influence of the angle θ on the damping peak and frequency enhancement in the BSC2 crystal in conf.1 as a function of temperature at constant applied field $B = 0.42$ T. A double-peak structure in damping accompanied with a frequency change is observed. We find that with increasing angle both peaks in damping shift to lower temperatures. As discussed above, this behavior indicates (1) the presence of two diffusion modes corresponding to two different length scales w_p (mode 1, high-temperature peak) and d_p (mode 3, low-temperature peak) for the penetration of the ac field (Fig. 3); (2) since $\rho(B, T_D, \theta)$ is determined only by the $B \sin\theta$ component [Eq. (10)], the constant resistivity criterion for the damping peak is fulfilled for both modes at lower temperatures at fixed field.

With increasing angle, the frequency change related to the low-temperature damping peak increases with respect to the higher temperature one as shown in Fig. 7. This can be understood as a crossover from a dominating shielding-current contribution in mode 1 to dominating elastic coupling in mode 3 with increasing angle. The relative change of the height of the damping peaks can be compared with the calculated total dissipation in mode 1 and mode 3. As shown by Brandt,[33] in each mode the time- and space-averaged linear dissipation per unit volume is given by

$$P = A(\omega B_i^2 \langle \phi^2 \rangle / 2\mu_0) \, | \, \mu''(\omega) \, | \, , \tag{14}$$

where $B_i = B\cos\theta$ for mode 1 and $B_i = B\sin\theta$ for mode 3. The prefactor is $A = (\pi w_p / 4d_p)$ for mode 1 and $A = 1$ for mode 3, and $\langle \phi^2 \rangle$ is the oscillation tilt angle squared and averaged over time. The imaginary part of the ac susceptibility μ'' is given by

$$\mu'' = \frac{\sinh(v) - \sin(v)}{v[\cosh(v) + \cos(v)]}, \tag{15}$$

where $v = (\omega l_i^2 \mu_0 / 2\rho)^{1/2}$, and $l_i = w_p$ for mode 1 or $l_i = d_p$ for mode 3. We assume from Eq. (10) that the resistivity $\rho^{\theta}_{a,b}(B, T, \theta)$ is given by

$$\rho^{\theta}_{a,b}(B, T, \theta) = \rho_0 \exp\left(\frac{-U_b\,(B\sin\theta, T)}{kT}\right), \tag{16}$$

where ρ_0 is chosen to be $10^5 \mu\Omega\,\mathrm{cm}$. Furthermore, we assume $U_b(B\sin\theta, T) \simeq U_b(B\sin\theta) f(T)$, where $f(T)$ accounts for the temperature dependence of the activation barrier,[50] and $U_b(B\sin\theta)$ is adjusted to match the peak temperatures. We have calculated the normalized dissipation and obtained a qualitative agreement between the experimental and calculated curves (see Fig. 7). Our calculations show a vanishing first peak at low angles. This

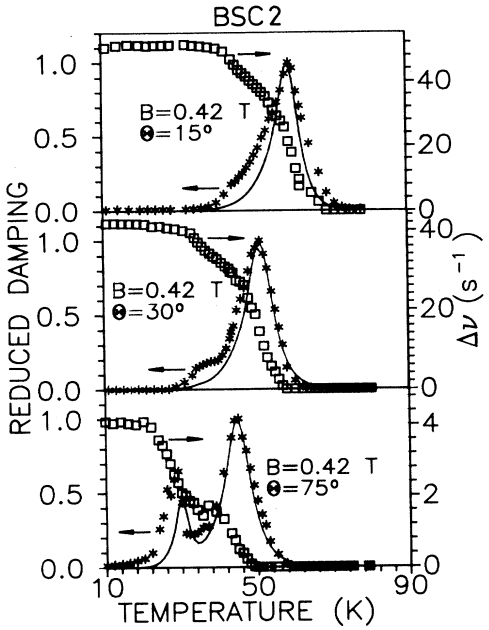

FIG. 7. Reduced damping and resonance-frequency enhancement as a function of temperature for the $Bi_2Sr_2CaCu_2O_{8+x}$ (BSC2) crystal measured in conf.1 at a fixed applied field at different angles θ. Maximum damping at $15°(30°, 75°) = 40.3\ \mathrm{s}^{-1}(36.4\ \mathrm{s}^{-1}, 2.2\ \mathrm{s}^{-1})$. The solid lines represent the normalized dissipation calculated with Eqs. (14)–(16).

is possibly due to an overestimation of demagnetization effects by the prefactor $A = \pi w_p/(4d_p)$.[54]

From a fit to the high-temperature damping peaks we obtain $U_b(B\sin\theta) = 630$ K, 750 K, 910 K at $B = 0.42$ T and $\theta = 15°$, 30°, 75°. These values match within 14% with those obtained from the slopes of the Arrhenius part of the resistivity data[55] on a 92- K $Bi_2Sr_2CaCu_2O_{8+x}$ single crystal (see also Sec. IV C).

We now show for both modes the scaling of the DL with the $B_i = B\sin\theta$ component measured for the BSC2 crystal. The temperatures corresponding to both damping peaks (see Fig. 7) obtained in the angular measurements in conf.1 are plotted as a function of field component perpendicular to the CuO_2 planes $B\sin\theta$ in Fig. 8. We observe that for each mode the reduced depinning temperatures T_D/T_c at different angles coalesce into a single DL. Similar scaling has been also reported in Refs. 29 and 56 using both vibrating-reed and ac-susceptibility measurements on a Bi 2:2:1:2 crystal. As discussed in Sec. III B within the diffusion picture, these two DL's should match the constant-resistivity lines. Taking the resonance frequency of the reed, $\nu = 1.2$ kHz, and using Eq. (9) with $l_i = d_p(w_p)$ for mode 3 (mode 1), we get for the lower and upper DL constant-ρ criteria of $6 \times 10^{-5} \mu\Omega\,\mathrm{cm}$ and $9.6 \times 10^{-2} \mu\Omega\,\mathrm{cm}$, respectively. In the same figure we compare these DL's with the respective constant in-plane resistivity lines taken from Ref. 55. The matching of both the DL's with constant-ρ lines is remarkable and establishes their origin in the finite ther-

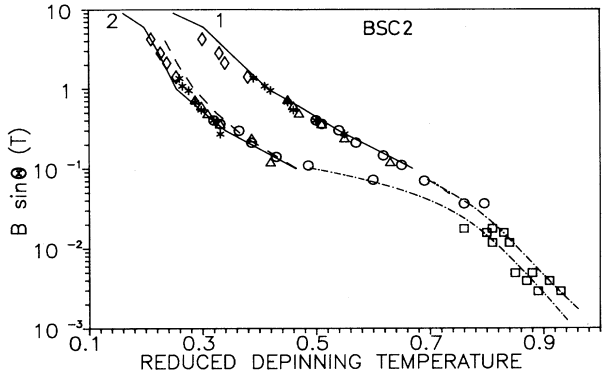

FIG. 8. Reduced depinning temperatures (T_D/T_c) for both diffusion modes of the $Bi_2Sr_2CaCu_2O_{8+x}$ (BSC2) crystal (BSC2) as a function of field component $\perp$ CuO_2 planes $B\sin\theta$, where θ is the angle between CuO_2 planes and the field B: ($\diamond$) 90°, ($*$) 75°, ($\triangle$) 60°, ($\bigcirc$) 45°, 30°, 15°, ($\square$) 2.6°, 1.4°, 0.4°. The solid lines are constant-resistivity $\rho^c_{a,b}$ lines corresponding to (1) $\rho = 9.6 \times 10^{-2}\mu\Omega\,\mathrm{cm}$ and (2) $6 \times 10^{-5}\mu\Omega\,\mathrm{cm}$ taken from Ref. 54. The dashed line represents a constant-resistivity line $\rho^c_c = 9.6 \times 10^{-2}\mu\Omega\,\mathrm{cm}$ taken from Ref. 47. The dashed-dotted lines are only a guide.

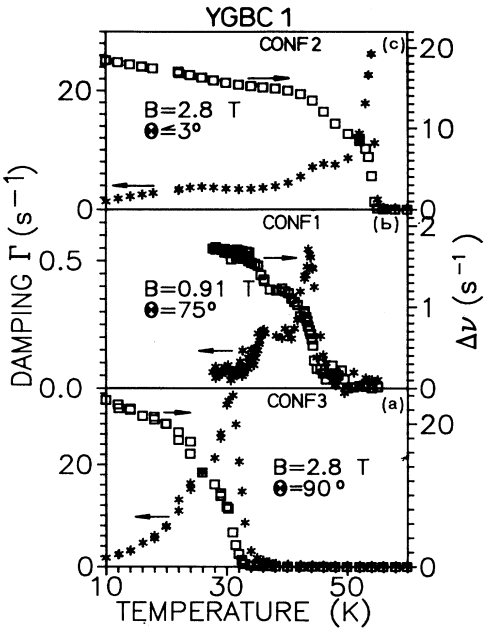

FIG. 9. Damping and resonance-frequency enhancement as a function of temperature for the Y(6% Gd)$Ba_2Cu_3O_{6.83}$ (YGBC1) crystal measured in (a) conf.3, (b) conf.1, and (c) conf.2 at different fixed applied fields and at different angles θ.

mally assisted flux-flow resistivity and the diffusive FLL motion.

In view of our extrapolation of the resistivity following an Arrhenius law to lower temperatures, we would like to make three remarks regarding the recently observed non-Arrhenius linear resistivity at low temperatures:[24] (1) The upper constant-resistivity line lies in the region where the resistivity is still Arrhenius like, (2) at the lowest measured temperatures the lower constant-resistivity line does not shift by more than 3% even if the non-Arrhenius behavior from Ref. 24 is taken into account, and (3) even if at low temperatures the FLL is in a vortex-glass state, the dissipation peaks in ac measurements can be well accounted for by two diffusion modes.

As mentioned in Sec. III B 1, if ρ^c_c would cause the penetration of the probing ac field in both mode 2 and mode 3, then three damping peaks should be observable. In conf.1 [Fig. 1(a)] there might be only a negligible ac field on the crystal face parallel to the y,z plane and mode 2 probably cannot be seen. If we consider the low-temperature peak due to mode 3 with a relevant dimension $l_3 = w_p$ and ρ^c_c as the relevant resistivity, the constant-resistivity ρ^c_c line (see dashed line in Fig. 8), taken from Ref. 47 measured on an 87-K Bi 2:2:1:2 crystal, also lies near the depinning line. Thus, to unambiguously prove the origin of mode 3, further measurements are needed on crystals with comparable width and thickness or on a crystal rotated in the x,z plane in conf.1.

2. *Y(6% Gd)$Ba_2Cu_3O_{6.83}$ single crystal*

Figure 9 shows the excess damping Γ and frequency enhancement $\Delta\nu$ as a function of temperature at constant applied field for the YGBC1 crystal in conf.2 ($\theta \leq 3°$ [Fig. 9(a)]), conf.1 ($\theta = 75°$ [Fig. 9(b)]) and conf.3 ($\theta \simeq 90°$ [Fig. 9(c)]). Similar to the Bi-based system, the observation of two peaks in the damping accompanied by the corresponding shift in frequency confirms the presence of both modes in this low-oxygen-content YGBC1 system. The broad dissipation peak at $\sim 26\,\mathrm{K}$ in conf.2 [Fig. 9(a)] has been discussed in Ref. 25 and is not related with thermally activated depinning as the two high-temperature dissipation peaks.

The depinning temperatures corresponding to both modes in the YGBC1 crystal are plotted for all the measured angles as a function of $B\sin\theta$ in Fig. 10. We should mention here that the low-temperature peak due to mode 3 was too small to be resolved in conf.1 at 60° for most of the field values. This is the reason that in Fig. 10 only one T_D point is shown at 60° (mode 3, lower DL). Similar to the Bi-based system, for this low-oxygen-content Y 1:2:3 system the $T_{Di}(B,\theta)$ data coalesce onto a single DL for each of the modes. With the resonance frequency ($\nu = 0.65$ kHz) and the corresponding diffusion lengths d_p and w_p for the two modes, we obtain the constant-resistivity criteria of 3.3×10^{-5} and $3.3 \times 10^{-3}\mu\Omega\,\mathrm{cm}$, respectively. Constant in-plane resistivity lines, taken from Ref. 11 for a low-oxygen-content Y-based crystal, are also shown in the same figure. The mismatch of the DL's and constant-ρ lines might be due to different oxygen concentration in the two crystals compared. Another explanation for the mismatch of the lower DL, which needs further investigation, might be that in mode 3 the relevant resistivity is ρ^c_c instead of $\rho^c_{a,b}$.

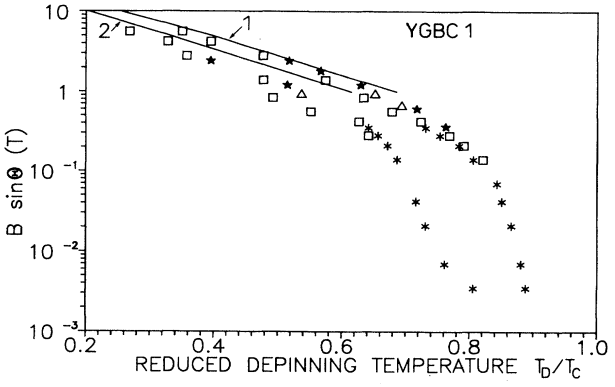

FIG. 10. Reduced depinning temperatures of the Y(6% Gd)$Ba_2Cu_3O_{6.83}$ (YGBC1) crystal as a function of the field component $\perp$ CuO_2 planes, $B\sin\theta$. For both diffusion modes: (□) 90°, (⋆) 75°, (△) 60°, (∗) 2.5°. The solid lines are constant-resistivity $\rho^c_{a,b}$ lines corresponding to (1) $\rho = 3.3 \times 10^{-3}\mu\Omega$ cm and (2) $3.3 \times 10^{-5}\mu\Omega$ cm taken from Ref. 11.

3. $YBa_2Cu_3O_7$ single crystal

Figure 11 shows the excess damping Γ and frequency enhancement $\Delta\nu$ as a function of temperature at a fixed field of 0.7 T applied at different angles θ for the YBC2 [Figs. 11(a) and 11(b)] and YBC1 [Fig. 11(c)] crystals in conf.1. The double-peak structure in damping is evident and confirms the presence of both modes in "3D-anisotropic" Y 1:2:3 superconductors. Note that the peaks are $\sim$ 4 K below T_c, i.e., at temperatures higher

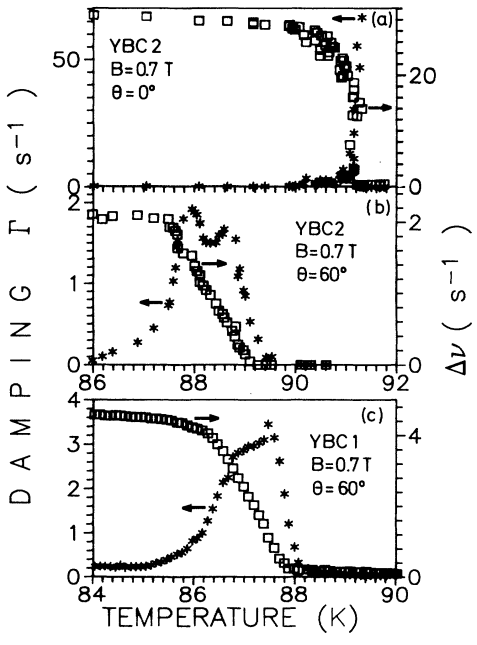

FIG. 11. Damping and resonance-frequency enhancement as a function of temperature for the $YBa_2Cu_3O_7$ crystals measured in conf.1 at a fixed applied field $B = 0.7$ T and at different angles θ. YBC2: (a) $\theta = 0°$, (b) 60°; YBC1: (c) $\theta = 60°$.

than any modest estimate of the 3D-2D superconductor crossover temperature $T_{2D} < T_c - 10$ K.[57] The smaller splitting of $\simeq 0.5$ K between the two modes is consistent with a smaller difference between the dimensions w_p and d_p of the crystal and the much steeper resistivity curves observed (i.e., larger activation barriers) for the "90-K" Y 1:2:3 superconductor.[11]

First, we discuss the observed depinning temperatures related with two modes within the 3D-anisotropic picture proposed by Brandt.[33] In Fig. 12 we plot the relative shift of both damping peak temperatures measured at a fixed field $B = 1.4$ T as a function of angle. Since the length L_p and width w_p for this crystal are the same, according to Sec. III B 2 mode 3.3 will be faster than mode 3.2 in the angle range $15° < \theta < 90°$. Using $w_p = 0.065$ cm, $d_p = 0.02$ cm for mode 3.3 and mode 3.1 in Eq. (12) [$\gamma = 7.6$ (Ref. 58)], from Eq. (13) we obtain the relevant in-plane resistivity at different angles. We interpolate the experimental resistivity data of fully oxygenated Y 1:2:3 (Ref. 11) to map out the expected temperature shift of the depinning peaks with angle for both modes (Fig. 12). The depinning lines calculated using resistivity data and the formulas for 3D-anisotropic superconductors described by Brandt are in fair agreement with our results. (Note that we are comparing our results with theory using the resistivity data of a different sample.) No reliable resistivity data has been found in the literature which could be used to obtain the angle dependence of T_D at $\theta < 15°$, the angle region where mode 3.2 should be faster than mode 3.3 and give rise to the dissipation peak. Within experimental error (±0.1 K in T_D) our data does not reveal a clear deviation of the DL at $\theta < 15°$ from the dependence observed at larger angles (Fig. 12).

The inset of Fig. 12 shows the measured temperature difference between the two damping peaks $T_{D,3.3} - T_{D,3.1}$

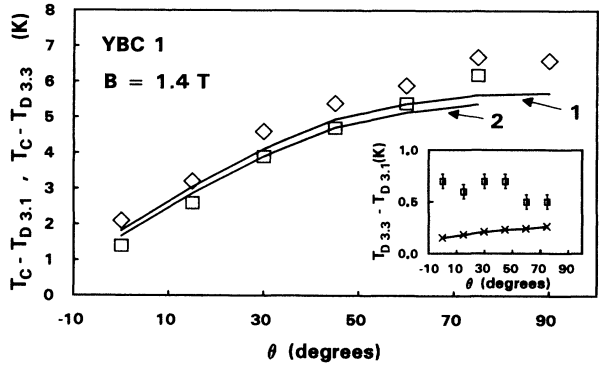

FIG. 12. Relative shift of the depinning peak temperatures $T_c - T_{D,3.3}$(□) and $T_c - T_{D,3.1}$(◇) as a function of the angle θ in a constant magnetic field $B = 1.4$ T for the YBC1 crystal. $T_{D,3.3}(T_{D,3.1})$ is the measured depinning temperature which corresponds to the diffusion mode 3.3 (3.1) [see Eqs. (11) and (12)]. The solid lines 1 and 2 are obtained from Eqs. (11) and (12) interpolating experimental data from Ref. 11. Inset: the temperature difference between the two depinning peaks as a function of angle θ at constant field. (□) measured difference at $B = 1.4$ T for YBC1 and (×) T_D(mode 3.3) $- T_D$(mode 3.1) calculated after Eqs. (11) and (12).

and the calculated one as a function of the angle between field and CuO_2 planes. Theory predicts a slightly smaller difference than measured. This difference as well as the temperature dependence of the damping at different angles and fields can be quantitatively understood taking into account slightly different diffusion lengths and demagnetization factors.[54]

Now we consider the scaling of the DL's for both observed modes in the whole range of the magnetic field. The depinning temperature obtained for different angles is shown as a function of $B\epsilon/\gamma$ in Fig. 13. We see a reasonable scaling of the depinning lines for both modes in all the measured angle range. The solid lines in Figs. 13(a) and 13(b) represent constant in-plane resistivity criteria of $1.8\times10^{-2}\mu\Omega$ cm and $5.6\times10^{-3}\mu\Omega$ cm obtained from Ref. 11, assuming the diffusion modes 3.3 and 3.1 for the upper and lower depinning lines. It should be noted that all the resistivity data used for comparison with vibrating reed measurements falls in the linear and Arrhenius resistivity region measured in Ref. 11.

C. Activation barrier in HTS's

In Fig. 14 we compare the activation barriers obtained from the slopes of the resistivity data from literature for all three high-temperature superconductors systems discussed above.

For Bi 2:2:1:2, the in-plane resistivity data ρ^c_{ab} of three different crystals measured in Refs. 10, 55, and 47, and ρ^c_c data of Ref. 47 has been used. Two results can be noted. First, within a 10% error of the extrapolation, the value of the activation barrier is approximately the same for all the crystals in spite of their different T_c's. This indicates that the activation barrier is not as sensitive to the oxygen content in the Bi 2:2:1:2 system as in the Y 1:2:3 system (see inset). Second, the activation barrier is independent of the direction of the current with respect to the point vortices in Bi 2:2:1:2 (see also Ref. 46).

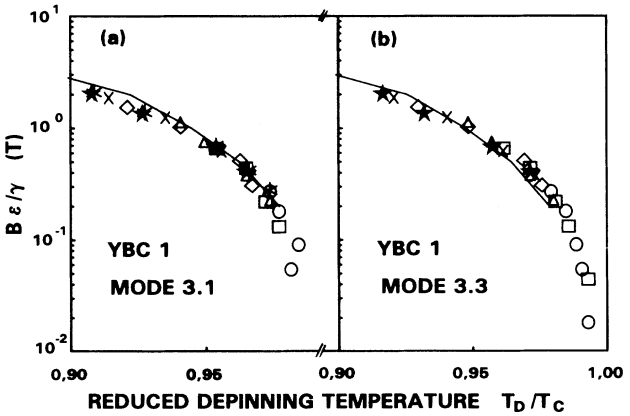

FIG. 13. Reduced depinning temperatures of the $YBa_2Cu_3O_7$ (YBC1) crystal (a) mode 3.1, (b) mode 3.3 as a function of the scaled field $B\epsilon/\gamma$. For both modes: (*) 90°, (⋆) 75°, (×) 60°, (◇) 45°, (△) 30°, (□) 15°, (○) 2°. The solid lines are constant-resistivity $\rho^c_{a,b}$ lines corresponding to (a) $\rho = 1.8\times10^{-2}\mu\Omega$ cm and (b) $5.6\times10^{-3}\mu\Omega$ cm taken from Ref. 11.

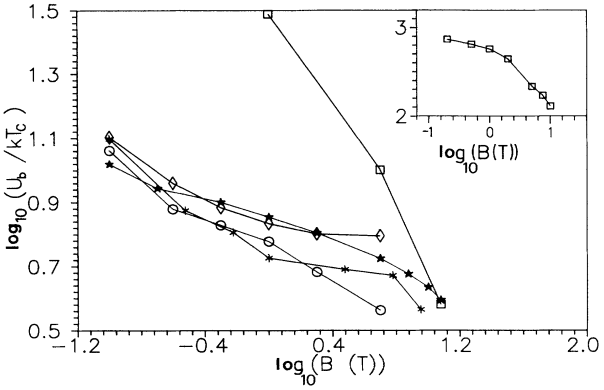

FIG. 14. Reduced activation barrier as a function of applied magnetic field ⊥ CuO_2 planes on a double-logarithmic scale, calculated from the slope of the Arrhenius plots of the resistivity taken from the literature. $Bi_2Sr_2CaCu_2O_{8+x}$: activation barrier from $\rho^c_{a,b}$ data: (Ref. 10) (⋆), (Ref. 24) (*), (Ref. 46) (○); ρ^c_c data of Ref. 46 (◇). Oxygen-deficient $YBa_2Cu_3O_7$: $\rho^c_{a,b}$ data of Ref. 11 (□). Inset: similar plot for fully oxygenated $YBa_2Cu_3O_7$: (□) $\rho^c_{a,b}$ data of Ref. 11.

As seen in Fig. 14, the reduced activation barriers for an oxygen-deficient Y 1:2:3 crystal are closer to those of Bi 2:2:1:2 in the whole measured field region, rather than to fully oxygenated Y 1:2:3. These results confirm a 2D-like scaling of T_D as we have experimentally observed.

V. REED-AMPLITUDE DEPENDENCE OF THE DEPINNING CROSSOVER

In this section we show the amplitude dependence of the depinning crossover measured in Conf.3 ($B \perp CuO_2$ planes) on all three single crystals BSC1, YGBC1, and YBC1. In anticipation of the results, we stress that no amplitude dependence was found at the depinning peak for the BSC1 and fully oxygenated YBC1 crystals.

A. $Bi_2Sr_2CaCu_2O_{8+x}$ single crystal

Figures 15 and 16 show the damping Γ and frequency change $\Delta\nu$ as a function of temperature measured at constant magnetic field $B \perp CuO_2$ planes at different amplitudes ϕ for the BSC1 crystal. In the measured amplitude range and for all values of the field three important observations can be pointed out: (1) There is no shift in the damping peak positions with amplitude; (2) at temperatures just below the peak and for all temperatures above the peak no amplitude dependence of the damping is observed; (3) at lower temperatures, however, there is a significant amplitude dependence of the damping. According to the TAFF model[18,19,59] the expected behavior of the FLL in a Bi 2:2:1:2 single crystal for $B \perp CuO_2$ planes is determined by its plastic deformations which give rise to a finite activation energy

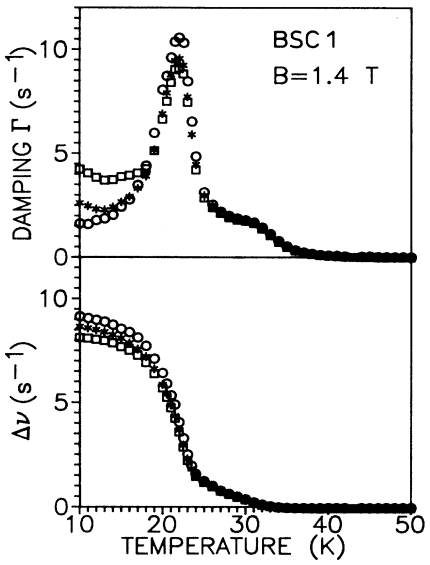

FIG. 15. Damping and resonance-frequency enhancement for the $Bi_2Sr_2CaCu_2O_{8+x}$ (BSC1) crystal measured with $B \perp CuO_2$ planes (conf.3) at fixed field for driving forces F/F_{min}: (○) 1, (*) 4; (□) 8. F is proportional to the square of the driving voltage.

even for vanishing currents. The results (1) and (2) support this model, since the dissipation due to vortex motion should be driving force independent as well as the constant-resistivity or depinning line should be independent of current or driving force in the linear (Ohmic) resistivity regime. The result (3) indicates a nonlinear (hysteretic) damping which can be related with the amplitude dependence of the coupling;[28,42] i.e., the pinning force does not depend linearly on FLL displacement, a behavior also seen in conventional superconductors.[38,60]

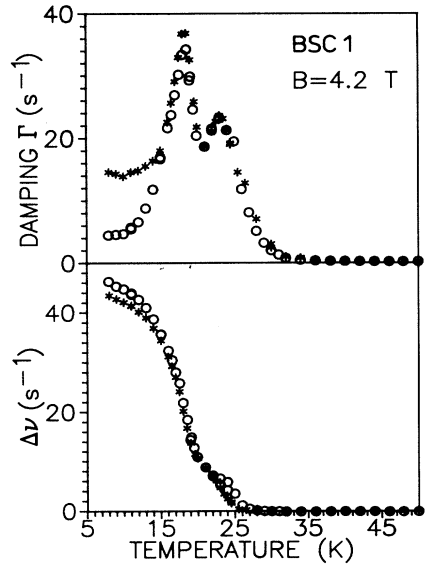

FIG. 16. Damping and resonance-frequency enhancement for the $Bi_2Sr_2CaCu_2O_{8+x}$ (BSC1) crystal for driving forces F/F_{min}: (○) 1, (*) 8 ($B \perp CuO_2$ planes, conf.3). F is proportional to the square of the driving voltage.

At lower temperatures, the decrease of $\Delta\nu$ with increasing amplitude (Fig. 13) reveals a decrease of the elastic coupling α, consistent with the increase of damping. At higher temperatures, $\Delta\nu(T)$ becomes amplitude independent, which is consistent with viscous damping.

B. Y(6% Gd)$Ba_2Cu_3O_{6.83}$ single crystal

Similar measurements of frequency enhancement and damping on the YGBC1 single crystal in conf.3 for $B \perp CuO_2$ planes are depicted in Fig. 17. In contrast to the Bi 2:2:1:2 crystal, this crystal shows an amplitude dependence of damping both below and at the peak. The dissipation peak shifts slightly to lower temperatures with increasing driving force. Both the shift of the peak temperature and the amplitude dependence of damping are not expected within the linear-resistivity model and cannot be understood at present. Possibly, an amplitude-dependent parameter α combined with a distribution of activation barriers could account for the observed amplitude dependence at the depinning line.

C. $YBa_2Cu_3O_7$ single crystal

Figure 18 shows Γ and $\Delta\nu$ as a function of temperature measured at different amplitudes for the YBC1 crystal and at $B = 2.8$ T. Within the error of the measurement, we found no amplitude dependence of the damping peaks as expected within the TAFF model.

VI. NOVEL DISSIPATION FEATURES IN Y- AND BI-BASED SUPERCONDUCTORS: MELTING LINES

Recently published measurements with a low-frequency torsional oscillator and in a twin-free Y-based

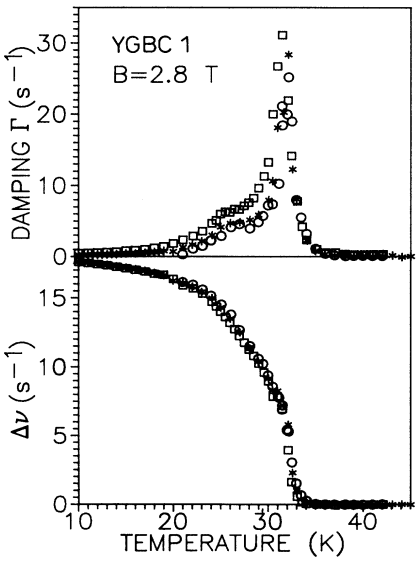

FIG. 17. Damping and resonance-frequency enhancement for the Y(6% Gd)$Ba_2Cu_3O_{6.83}$ (YGBC1) crystal measured with $B \perp CuO_2$ planes (conf.3) at fixed field for F/F_{min}: (○) 1, (*) 4 , (□) 8.

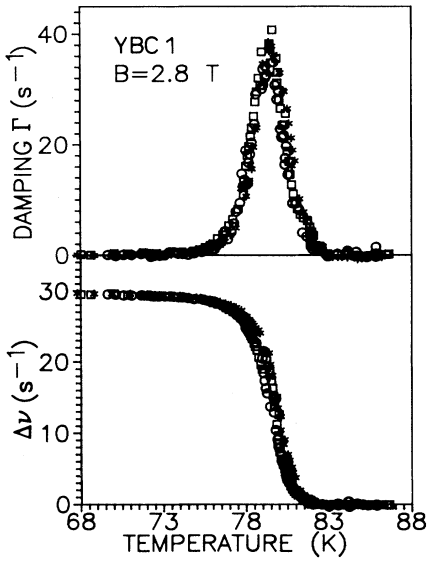

FIG. 18. Damping and resonance-frequency enhancement for the $YBa_2Cu_3O_7$ (YBC1) crystal measured with $B \perp CuO_2$ planes (conf.3) at fixed field for driving forces F/F_{min}: (*) 1, (○) 4, (□) 8.

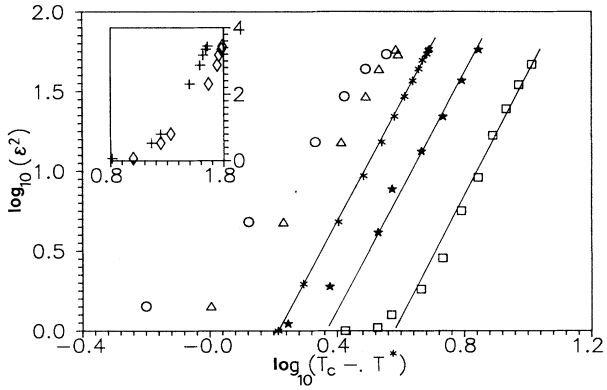

FIG. 19. Double-logarithmic plot of $T_c - T^*$ vs $\epsilon^2 = \cos^2\theta + \gamma^2 \sin^2\theta$. T^* means (*) melting temperatures of a $YBa_2Cu_3O_7$ untwinned single crystal at a fixed field of 2 T from the low-frequency torsional oscillator experiment of Ref. 23. Temperatures at constant-resistivity lines (□) $0.6\mu\Omega$ cm and (*) $10\mu\Omega$ cm at a fixed field of 6 T in a single-crystal thin film of $YBa_2Cu_3O_7$ from Ref. 61. (△) and (○) are the two damping peak temperatures corresponding to both diffusion modes at a fixed field of 1.4 T for $YBa_2Cu_3O_7$ (YBC1) crystal measured in this work; for clarity the data points are shifted by 0.05 units to the left. Inset: similar plots for $Bi_2Sr_2CaCu_2O_{8+x}$ (BSC2) crystal; (+) and (◇) are the two damping temperatures corresponding to both diffusion modes at a fixed field of 0.42 T measured in this work. Solid lines are only a guide to the eye.

HTS reported evidence for flux-lattice melting in the reversible B-T region.[23,27] It has been pointed out that the anomalous peak in the damping at a characteristic peak temperature "$T_m(B)$" shows an angle dependence as $\epsilon^2 = \cos^2\theta + \gamma^2 \sin^2\theta$,[48] which was taken as strong evidence for a melting transition of the FLL.[23] We note, however, that a similar scaling is also followed by the constant-resistivity criterion data and the thermally activated depinning peaks observed by the vibrating-reed measurements in twinned Y-based HTS crystals.

Figure 19 shows constant-resistivity lines for $YBa_2Cu_3O_7$ crystals versus ϵ^2 at $B = 6$ T using the data of Ref. 61, along with the melting temperatures taken from Ref. 23. The damping peak temperatures of YBC1 at $B = 1.4$ T are also included for both modes in the same figure. It is clear that within the scatter of the data all lines have the same slope above $\theta \geq 10°$. This suggests that any constant-resistivity line in Y 1:2:3 scales with ϵ^2. Therefore, such scaling alone cannot be used as a criterion for melting. Note that the resistivity data in Ref. 61 were taken on single-crystal thin films with higher pinning. A similar plot of the damping peak temperatures for both modes of the BSC1 crystal reveals steeper slopes than for the Y 1:2:3 system (see inset of Fig. 19).

At present we are performing highly sensitive measurements of the dissipation below the depinning in $YBa_2Cu_3O_7$ crystals at different angles between the field and CuO_2 planes. Preliminary results indicate that an anomalous enhancement of the elastic pinning force occurs at temperatures lower than the $T_D(B)$ lines, i.e., in the irreversible region. The anomaly is also seen as a decrease in the damping and depends on the magnetic history of the crystal.[62] Although the anomaly has the same field dependence as reported in Refs. 23 and 27 for the melting temperature, it weakens clearly at angles larger than 15°. An analysis of the data within a melting theory is under way and will be published elsewhere.[62]

As reported recently,[25] a third dissipation peak is observed at a lower temperature T_x for the YGBC1 ($T_x \simeq 26$ K) and both BSC1 and BSC2 ($T_x \simeq 30$ K) crystals for angles $\theta \leq 3°$. The temperature T_x is nearly field independent for BSC1, BSC2, and YGBC1.[25] dc magnetization measurements reported recently on a $Bi_2Sr_2CaCu_2O_{8+x}$ crystal provide additional evidence for a phase transition of the FLL at temperatures much lower than the irreversibility line.[26] More work is needed to fully comprehend the nature of these features and the properties of "Josephson vortices" in high-temperature superconductors.

VII. CONCLUSIONS

In this work we have given a quantitative understanding of the origin of frequency enhancement in a vibrating combination of host reeds with an attached superconducting crystal. Depending on the pinning strength α, dimensions of the crystal, and the orientation of magnetic field, the origin of the restoring force can be due to the shielding currents (demagnetization effects), the tilt modulus c_{44}, or the Labusch parameter α itself. Conf.2 turns out to be an interesting geometry to study the properties of FL's || conducting planes in layered superconductors. In this configuration, our results indicate pinned

"Josephson vortices" through the substantial frequency enhancement with magnetic field for Bi 2:2:1:2 crystals.

For angles $0° < \theta < 90°$ we observe two damping peaks due to two diffusion modes for all five Bi 2:2:1:2, oxygen-deficient Y 1:2:3, and fully oxygenated Y 1:2:3 crystals. At $\theta = 90°$ we have shown that the damping peaks are amplitude independent for both Bi 2:2:1:2 and fully oxygenated Y 1:2:3 in complete agreement with the predictions of the TAFF model. The small deviations observed for oxygen-deficient Y(6% Gd)$Ba_2Cu_3O_{6.83}$ are not completely understood. The damping peak temperatures corresponding to both modes scale with $B \sin\theta$ down to the lowest measured angles in Bi 2:2:1:2 ($\theta \simeq 1°$) and oxygen-deficient Y 1:2:3 ($\theta \simeq 3°$), whereas for fully oxygenated Y 1:2:3 crystals a 3D-anisotropy approach is needed.

The rescaled depinning temperatures collapse on two curves and match the constant in-plane resistivity lines, consistent with the TAFF model for all three compounds. More work is needed to establish the role of ρ_c^c in the penetration of the ac field.

ACKNOWLEDGMENTS

We wish to acknowledge the collaboration of W. Ettig and U. Zschuppe, and L. Bauernfeind and W. Widder for the resistance measurements. This work was partially supported by the Bayerische Forschungstiftung under FORSUPRA. One of the authors (Y.K.) was supported by the DAAD.

* Present address: Département de Physique de la Matière Condensée, Université de Génève, Quai Ernest-Ansermet 24, CH-1211 Génève 4, Switzerland.

† Permanent address: A. F. Ioffe Physical-Technical Institute, St. Petersburg, Russia. Present address: University of Estadual de Campinas, 13081-970 Campinas, Brazil.

‡ Present Address: Phillips Communications Industries, Nürnberg, Germany.

[1] K. A. Müller, M. Takashige, and J. G. Bednorz, Phys. Rev. Lett. **58**, 1143 (1987).

[2] Y. Yeshurun and A. P. Malozemoff, Phys. Rev. Lett. **60**, 2202 (1988).

[3] P. L. Gammel, L. F. Schneemeyer, J. V. Waszczak, and D. J. Bishop, Phys. Rev. Lett. **61**, 1666 (1988); E. H. Brandt, P. Esquinazi, and G. Weiss, *ibid.* **62**, 2330 (1989); R. Kleiman *et al.*, *ibid.* **62**, 2331 (1989).

[4] A. P. Malozemoff, T. K. Worthington, Y. Yeshurun, F. Holtzberg, and P. H. Kes, Phys. Rev. B **38**, 7203 (1988).

[5] T. K. Worthington, A. P. Malozemoff, F. H. Holtzberg, G. V. Chandrashekhar, and P. Strobel (unpublished).

[6] J. van den Berg, C. J. van der Beek, P. H. Kes, J. A. Mydosh, M. J. V. Menken, and A. A. Menovsky, Supercond. Sci. Technol. **1**, 249 (1989).

[7] P. H. Kes, J. van den Berg, C. J. van der Beek, and J. A. Mydosh, Supercond. Sci. Technol. **1**, 242 (1989).

[8] A. Gupta, P. Esquinazi, H. F. Braun, and H.-W. Neumüller, Phys. Rev. Lett. **63**, 1869 (1989).

[9] A. Gupta, P. Esquinazi, H. F. Braun, W. Gerhäuser, H.-W. Neumüller, K. Heine, and J. Tenbrink, Europhys. Lett. **10**, 663 (1989).

[10] T. T. M. Palstra, B. Batlogg, L. F. Schneemeyer, and J. V. Waszczak, Phys. Rev. Lett. **61**, 1662 (1988).

[11] T. T. M. Palstra, B. Batlogg, R. B. van Dover, L. F. Schneemeyer, and J. V. Waszczak, Phys. Rev. B **41**, 6621 (1990).

[12] P. Esquinazi, Solid State Commun. **74**, 75 (1990).

[13] E. H. Brandt, Z. Phys. B **80**, 167 (1990).

[14] J. Pankert, Physica C **168**, 335 (1990).

[15] J. Pankert, G. Marbach, A. Comberg, P. Lemmens, P. Frönig, and S. Ewert, Phys. Rev. Lett. **65**, 3052 (1990).

[16] M. P. A. Fischer, Phys. Rev. Lett. **62**, 1415 (1989).

[17] M. V. Feigel'man, V. B. Geshkenbein, A. I. Larkin, and V. M. Vinokur, Phys. Rev. Lett. **63**, 2303 (1989).

[18] M. V. Feigel'man, V. B. Geshkenbein, and A. I. Larkin, Physica C **167**, 177 (1990).

[19] V. M. Vinokur, P. H. Kes, and A. E. Koshelev, Physica C **168**, 29 (1990).

[20] B. I. Ivlev and N. B. Kopnin, J. Low Temp. Phys. **80**, 161 (1990).

[21] E. H. Brandt, Int. J. Mod. Phys. B **5**, 751 (1991).

[22] K. H. Fischer, Physica C **178**, 161 (1991).

[23] R. G. Beck, D. E. Farrell, J. P. Rice, D. M. Ginsberg, and V. G. Kogan, Phys. Rev. Lett. **68**, 1594 (1992).

[24] H. Safar, P. L. Gammel, D. J. Bishop, D. B. Mitzi, and A. Kapitulnik, Phys. Rev. Lett. **68**, 2672 (1992).

[25] Y. Kopelevich, A. Gupta, and P. Esquinazi, Phys. Rev. Lett. **70**, 666 (1993).

[26] H. Pastoriza, F. de la Cruz, D. B. Mitzi, and A. Kapitulnik, Phys. Rev. B **46**, 9278 (1992).

[27] G. D'Anna, W. Benoit, W. Sadowski, and E. Walker, Europhys. Lett. **20**, 167 (1992).

[28] P. Esquinazi, J. Low Temp. Phys. **85**, 139 (1991).

[29] C. Durán, J. Yazyi, F. de la Cruz, D. Bishop, D. Mitzi, and A. Kapitulnik. Phys. Rev. B **44**, 7737 (1991).

[30] Y. Kopelevich, A. Gupta, P. Esquinazi, C.-P. Heidmann, and H. Müller, Physica C **183**, 345 (1991).

[31] H. Drulis, Z. Xu, J. Brill, L. de Long, and J.-C. Hou, Phys. Rev. B **44**, 4731 (1991); Physica C **202**, 256 (1992).

[32] A. Swanson *et al.* (unpublished).

[33] E. H. Brandt, Phys. Rev. Lett. **68**, 3769 (1992).

[34] P. H. Kes, J. Aarts, V. M. Vinokur, and C. J. van der Beek, Phys. Rev. Lett. **64**, 1063 (1990).

[35] Y. Iye, S. Nakamura, and T. Tamegai, Physica C **174**, 227 (1991).

[36] H. Raffy, S. Labdi, O. Laborde, and P. Monceau, Phys. Rev. Lett. **66**, 2515 (1991).

[37] R. Fastampa, M. Giura, R. Marcon, and E. Silva, Europhys. Lett. **18**, 75 (1992).

[38] P. Esquinazi, H. Neckel, G. Weiss, and E. H. Brandt, J. Low Temp. Phys. **64**, 1 (1986).

[39] D. Shaltiel, S. E. Barnes, H. Bill, M. Francois, H. Hagemann, J. Jegondaz, D. Lovy, P. Monod, M. Peter, A. Revcolevschi, W. Sadowaski, and E. Walker, Physica C **161**, 441 (1988).

[40] F. I. Schulz, Diploma thesis, University of Bayreuth, 1991.
[41] P. Fischer, Physica C **196**, 105 (1992).
[42] E. H. Brandt, P. Esquinazi, and H. Neckel, J. Low Temp. Phys. **63**, 187 (1986).
[43] J. Kober, A. Gupta, P. Esquinazi, H. F. Braun, and E. H. Brandt, Phys. Rev. Lett. **66**, 2507 (1991).
[44] A. Gupta, Ph.D. thesis, University of Bayreuth, 1991.
[45] E. H. Brandt and A. Sudbø, Physica C **180**, 426 (1991).
[46] Yu. I. Latyshev and A. F. Volkov, Physica C **182**, 47 (1991).
[47] R. Busch, G. Ries, H. Werthner, G. Kreiselmeyer, and G. Saemann-Ischenko, Phys. Rev. Lett. **69**, 522 (1992).
[48] G. Blatter, V. B. Geshkenbein, and A. I. Larkin, Phys. Rev. Lett. **68**, 875 (1992).
[49] Y. Iye, I. Oguro, T. Tamegai, W. R. Datars, N. Motohira, and K. Kitazawa, Physica C **199**, 154 (1992).
[50] A. Gupta, P. Esquinazi, H. F. Braun, W. Sadowski, E. Walker, and D. Shaltiel, Bull. Mater. Res. (India) **14**, 877 (1991).
[51] A. Sudbø and E. H. Brandt, Phys. Rev. Lett. **66**, 1781 (1991).
[52] See, for example, N. Chikumoto *et al.*, Physica C **199**, 32 (1992).
[53] L. N. Bulaevskii, M. Ledvij, and V. G. Kogan, Phys. Rev. B **46**, 366 (1992).
[54] M. Ziese and P. Esquinazi (unpublished).
[55] J. W. P. Hsu, D. B. Mitzi, A. Kapitulnik, and M. Lee, Phys. Rev. Lett. **67**, 2095 (1991).
[56] J. Yazyi, A. Arribére, C. Durán, F. de la Cruz, D. Mitzi, and A. Kapitulnik, Physica C **184**, 524 (1991).
[57] D. E. Farrell, S. Bonham, J. Foster, Y. C. Chang, P. Z. Jiang, K. G. Vandervoort, D. J. Lam, and V. G. Kogan, Phys. Rev. Lett. **63**, 782 (1989).
[58] D. E. Farrel, J. P. Rice, and D. M. Ginsberg, Phys. Rev. Lett. **67**, 1165 (1991).
[59] C. J. Van der Beek and P. H. Kes, Phys. Rev. B **43**, 13 032 (1991).
[60] P. Esquinazi and E. H. Brandt, Jpn. J. Appl. Phys. **26**, 1513 (1987).
[61] Y. Iye, T. Terashima, and Y. Bando, Physica C **177**, 393 (1991).
[62] M. Ziese, A. Gupta, P. Esquinazi, P. Fischer, and H. F. Braun (unpublished).